Protein aggregation of the p63 transcription factor underlies severe skin fragility in AEC syndrome

Claudia Russo[a,1], Christian Osterburg[b,1], Anna Sirico[a,1], Dario Antonini[c,d], Raffaele Ambrosio[d], Julia Maren Würz[b], Jörg Rinnenthal[b,2], Marco Ferniani[c], Sebastian Kehrloesser[b,3], Birgit Schäfer[b], Peter Güntert[b], Satrajit Sinha[e], Volker Dötsch[b,4,5], and Caterina Missero[a,c,4,5]

[a]Centro di Ingegneria Gentica e Biotecnologie Avanzate, 80145 Naples, Italy; [b]Institute of Biophysical Chemistry and Center for Biomolecular Magnetic Resonance, Goethe University, 60438 Frankfurt, Germany; [c]Department of Biology, University of Naples Federico II, 80126 Naples, Italy; [d]Istituto di Ricovero e Cura a Carattere Scientifico (IRCCS) Istituto di Ricerca Diagnostica e Nucleare (SDN), 80143 Naples, Italy; and [e]Department of Biochemistry, Center of Excellence in Bioinformatics and Life Sciences, State University of New York, Buffalo, NY 14203

Edited by Carol Prives, Columbia University, New York, NY, and approved December 18, 2017 (received for review August 21, 2017)

The *p63* gene encodes a master regulator of epidermal commitment, development, and differentiation. Heterozygous mutations in the C-terminal domain of the *p63* gene can cause ankyloblepharon-ectodermal defects-cleft lip/palate (AEC) syndrome, a life-threatening disorder characterized by skin fragility and severe, long-lasting skin erosions. Despite deep knowledge of p63 functions, little is known about mechanisms underlying disease pathology and possible treatments. Here, we show that multiple AEC-associated p63 mutations, but not those causative of other diseases, lead to thermodynamic protein destabilization, misfolding, and aggregation, similar to the known p53 gain-of-function mutants found in cancer. AEC mutant proteins exhibit impaired DNA binding and transcriptional activity, leading to dominant negative effects due to coaggregation with wild-type p63 and p73. Importantly, p63 aggregation occurs also in a conditional knock-in mouse model for the disorder, in which the misfolded p63 mutant protein leads to severe epidermal defects. Variants of p63 that abolish aggregation of the mutant proteins are able to rescue p63's transcriptional function in reporter assays as well as in a human fibroblast-to-keratinocyte conversion assay. Our studies reveal that AEC syndrome is a protein aggregation disorder and opens avenues for therapeutic intervention.

AEC syndrome | mouse model | p63 | protein aggregation | skin

As a tetrameric transcription factor required for the development of stratified epithelia, p63 plays an essential role in the commitment of simple ectoderm to epidermal lineages and in the proliferative potential of epidermal stem cells (1–6). Its DNA binding domain (DBD) is highly homologous to the DBD of its family members, p53 and p73. Therefore, p63 binds to canonical p53 DNA-binding sites and shares some biological functions with the other members of the family (7, 8). The highly conserved oligomerization domain (OD) allows homotetramerization required for high DNA affinity (9), and hetero-tetramerization with p73 (10, 11). Due to the presence of two independent promoters, two classes of p63 proteins are expressed that differ at the amino (N)-terminus: TAp63 and ΔNp63. TAp63 protein is highly expressed in a dimeric inactive conformation in female germ cells during meiotic arrest (12, 13). DNA damage promotes the formation of active tetramers (9), leading to DNA damage-induced oocyte death (12). In contrast, the ΔNp63 proteins are found in a tetrameric form, and are primarily expressed in the basal regenerative layers of the epidermis and other stratified epithelia, where they play multiple essential roles in keratinocyte proliferation, differentiation, and cell adhesion (3, 5, 7, 14, 15). For most epidermal target genes, ΔNp63 acts as a transactivator, but it can also act as a repressor for other genes (3, 5, 16–19).

At least three distinct 3′ splice variants also exist: α, β, and γ. The α isoform is by far the most abundant isoform in stratified epithelia and contains a poorly characterized sterile-α-motif (SAM) domain, a putative protein interaction module present in a wide variety of proteins, and a post-SAM (PS) domain. The p63 SAM domain shows a typical five-helix bundle architecture (20, 21), is unable to form homodimers (21, 22), and its function remains unknown. The PS domain is about the same length as the SAM domain and can be divided in two subdomains. The N-terminal subdomain (45 amino acids) contains a transcriptional inhibitory (TI) sequence that forms a closed inactive dimer with the TA domain (23, 24). The C-terminal subdomain (25 amino acids) contains a sumoylation site involved in regulating p63's concentrations (24).

Heterozygous mutations in *p63* (*TP63*) are causative of a group of autosomal dominant human disorders characterized by various combinations of ectodermal dysplasia, orofacial clefting, and limb malformations (7, 25). Among these disorders, ectrodactyly, ectodermal dysplasia, and cleft lip/palate syndrome [EEC, Online Mendelian Inheritance in Man (OMIM) 604292] is mainly characterized by severe ectrodactyly and limb defects (26), whereas in ankyloblepharon-ectodermal defects-cleft lip/palate syndrome

Significance

The *p63* gene encodes a master regulator of epidermal development and function. Specific mutations in *p63* are causative of a life-threatening disorder mainly characterized by severe skin erosions and cleft palate. Little is known about the mechanisms underlying disease pathology and possible treatments. Based on biochemical studies, genetic mouse models, and functional assays, we demonstrate that these mutations cause p63 protein misfolding and aggregation. Protein aggregation lead to reduced DNA binding and impaired transcriptional activity. Importantly, genetic modifications of *p63* that abolish aggregation of the mutant proteins rescue its function, revealing that ankyloblepharon-ectodermal defects-cleft lip/palate syndrome is a protein aggregation disorder and opening avenues for therapeutic intervention.

Author contributions: V.D. and C.M. designed research; C.R., C.O., A.S., D.A., R.A., J.M.W., J.R., M.F., S.K., B.S., P.G., and S.S. performed research; C.R., C.O., A.S., D.A., V.D., and C.M. analyzed data; and C.R., C.O., A.S., D.A., V.D., and C.M. wrote the paper.

The authors declare no conflict of interest.

This article is a PNAS Direct Submission.

Data deposition: The NMR chemical shifts have been deposited in the Protein Data Bank, www.wwpdb.org (PDB ID code 5N2O).

[1]C.R., C.O., and A.S. contributed equally to this work.

[2]Present address: Boehringer Ingelheim RCV GmbH & Co KG, A-1121 Vienna, Austria.

[3]Present address: Cancer Research UK, Cambridge Institute, Li Ka Shing Centre, University of Cambridge, Cambridge CB2 0RE, United Kingdom.

[4]V.D. and C.M. contributed equally to this work.

[5]To whom correspondence may be addressed. Email: vdoetsch@em.uni-frankfurt.de or missero@ceinge.unina.it.

This article contains supporting information online at www.pnas.org/lookup/suppl/doi:10.1073/pnas.1713773115/-/DCSupplemental.

(AEC, OMIM 106260), the distinguishing features are ankyloblepharon, congenital erythroderma, skin fragility, atrophy, palmoplantar hyperkeratosis, and extensive skin erosions (21, 27). Distinct *p63* mutations can also cause nonsyndromic diseases, including isolated split hand/foot malformation (SHFM4, OMIM 605289) (28). For each of these diseases, mutations are generally clustered in specific p63 protein domains or are found in the same domain but have distinct characteristics, suggesting a genotype-to-phenotype correlation (25) (Fig. 1*A*). AEC syndrome mutations are predominantly clustered in the C-terminal portion of p63, either as missense mutations in the SAM domain and more rarely in the TI domain, or as single-base frameshift mutations that lead to elongation of the C-terminal domain (25).

It is generally believed that heterozygous *p63* mutations have a dominant-negative effect due to formation of mixed wild-type and mutant p63 tetramers, reducing the cellular amounts of functional p63. The fact that different mutations give rise to distinct phenotypes and syndromes, however, suggests distinct mechanisms of action of the mutants. Here, we report that the dominant-negative activity effects of AEC-associated *p63* mutations result from an increased aggregation propensity. Mutant p63 induces misfolding and coaggregation of wild-type p63, causing partial impairment in DNA binding and deficient transcription of target genes. This is observed both in heterologous cells expressing AEC mutant p63 proteins and in keratinocytes derived from a newly developed conditional knock-in mouse model for AEC syndrome. Mutant p63 also leads to coaggregation with its paralogue p73, possibly also leading to its inactivation. Relieving mutant p63 aggregation leads to reactivation of its function, indicating that aggregation is the cause of its impairment.

Results

Aggregation Is a Characteristic Feature of AEC Mutant p63 Proteins. AEC mutations cluster predominantly in the carboxyl (C) terminus of the p63α isoform and include several missense mutations in the SAM domain (e.g., L514F, G530V), two missense mutations in the TI domain (R598L, D601V), and several frameshift mutations leading to abnormal extensions of the C terminus (e.g., 3′ss intron 10, 1456InsA, 1709DelA, 1859DelA) (Fig. 1*A*). In contrast, the few EEC mutations found in the C terminus cause a premature stop codon (Fig. 1*A*), suggesting that missense mutations, extensions, or truncations of the C terminus differentially alter p63 function. The mechanisms by which AEC-causative mutations interfere with p63 functions has remained obscure, and we hypothesized that a selective structural alteration may be at the basis of this disorder. To test this hypothesis, we first determined the structure of L514F mutant SAM domain using NMR (Fig. 1*B* and *SI Appendix*, Fig. S1*A* and Table S1). L514 is a highly conserved amino acid in the first helix of the SAM domain, which is mutated to phenylalanine, serine, or valine in AEC patients (21, 29). The wild-type and L514F mutant structures revealed close similarity, with a backbone root mean square deviation (rmsd) value of 1.5 Å. The less compact fold of the mutant protein was caused by steric clashes due to the placement of the phenylalanine side chain in the hydrophobic core as previously predicted (30), likely leading to destabilization of the SAM domain.

To measure SAM domain destabilization, we monitored temperature-induced unfolding by circular dichroism (CD) spectroscopy (Fig. 1*C*). While the wild-type SAM domain showed a melting temperature of 79 °C, the mutant was destabilized with an unfolding temperature of 65 °C. In addition, only the unfolding of the wild-type SAM domain was reversible, while the L514F SAM domain mutant irreversibly precipitated upon unfolding (Fig. 1*D* and *SI Appendix*, Fig. S1*B*).

To investigate whether AEC mutants might be prone to destabilization and precipitation due to an increased aggregation propensity, we analyzed the p63 amino acid sequence using the TANGO algorithm that predicts aggregation prone regions (APRs) in proteins (31). This analysis indicated that two peptides (peptides 1 and 2), located in the first and third helix of the SAM domain, displayed some aggregation propensity, which was enhanced by the L514F and G530V mutations, respectively (Fig. 1*E*, *Lower* and *SI Appendix*, Fig. S1*C* and Table S2). Similarly, the two point mutations within the TI domain, R598L and D601V, strongly enhanced the low intrinsic aggregation propensity of the TI domain (Fig. 1*E*, *Lower* and *SI Appendix*, Table S2). Finally, TANGO analysis was performed for 3′ss-int10 and 1456InsA, and on the 1709DelA and 1859DelA mutants that lead to frameshifts and two different extensions of the C terminus, respectively. Aberrant elongations of the mutant proteins generated APRs (peptides I, II, III) (Fig. 1*E* and *SI Appendix*, Fig. S1*D* and Table S2). In contrast, EEC-associated frameshift mutations in the C terminus 1572InsA, 1576DelTT, and 1743DelAA did not create new peptides predicted to lead to aggregation (*SI Appendix*, Table S2), suggesting that the generation, exposure, or enhancement of APRs is a characteristic feature of AEC syndrome.

To assess whether AEC-associated mutant p63 proteins have the propensity to form aggregates in mammalian cells, wild-type and mutant p63 were overexpressed in H1299 cells that are devoid of p53 and its family members, and run on Blue-Native polyacrylamide gel electrophoresis (BN-PAGE) followed by Western blotting. Transiently overexpressed wild-type p63 and EEC mutations (R304Q, 1576DelTT, 1743DelAA, 1572InsA) run primarily as monomers (Fig. 1*F*), in agreement with the short half-life of the p63 tetramer compared with that of other p53 family members (32). In contrast, overexpression of p63L514F and all other tested AEC mutants caused a shift in molecular mass, consistent with the formation of large multimeric assemblies (Fig. 1*F*). Such aggregation was similar to that observed for the conformation mutant of p53 (R175H), known to be destabilized and to aggregate (33), whereas the p53 DNA contact mutant R248W did not aggregate (*SI Appendix*, Fig. S1*E*). Similar results were obtained by size exclusion chromatography (SEC), in which most of the p63L514F mutant protein eluted at high molecular weight (Fig. 1*G*) similarly to p53R175H mutant protein (*SI Appendix*, Fig. S1*G*), whereas wild-type p63 eluted at low molecular weight.

AEC Mutant p63 Selectively Binds to p53 Family Members. The oncogenic gain-of-function activities attributed to mutant p53 have been correlated to aberrant binding and coaggregation with wild-type p63 and p73 (33). We previously reported that binding of p53 mutants to p63 is dependent on the low but detectable aggregation tendency of the p63 TI domain (Fig. 1*E* and *SI Appendix*, Table S2) (32). Such aggregation tendency is completely abolished by the p63V603D mutant that is unable to bind p53 (32). To test whether the aggregation propensity of AEC mutants in the SAM domain is dependent on the mild intrinsic aggregation propensity of the TI domain, we tested AEC mutants in the background of the V603D mutation. All AEC mutants in the SAM domain exhibited severe aggregation even in the V603D background, while the wild-type and EEC mutants (R279H, R304Q) displayed no residual aggregation as shown by BN-PAGE and SEC (Fig. 2 *A* and *B*). Accordingly, AEC-associated mutants strongly bound to mutant p53 even in the V603D background, whereas no binding was observed for EEC mutants (Fig. 2*C*). Aggregation of AEC mutants was temperature-dependent, as p63L514F/V603D aggregation progressively increased at physiological temperature, whereas no aggregation was observed in either p63V603D or p63R304Q/V603D even at high temperature (*SI Appendix*, Fig. S2*A*). Taken together, these data indicate that AEC mutants have a strong tendency of aggregating, and that AEC mutations in the SAM domain cause aggregation independently of the TI domain.

To investigate whether AEC-associated mutant p63 may coaggregate with wild-type p63, we cotransfected HA-tagged wild-type p63 with Myc-tagged wild-type or AEC mutant p63. Interestingly, even in the V603D background, the SAM domain mutant

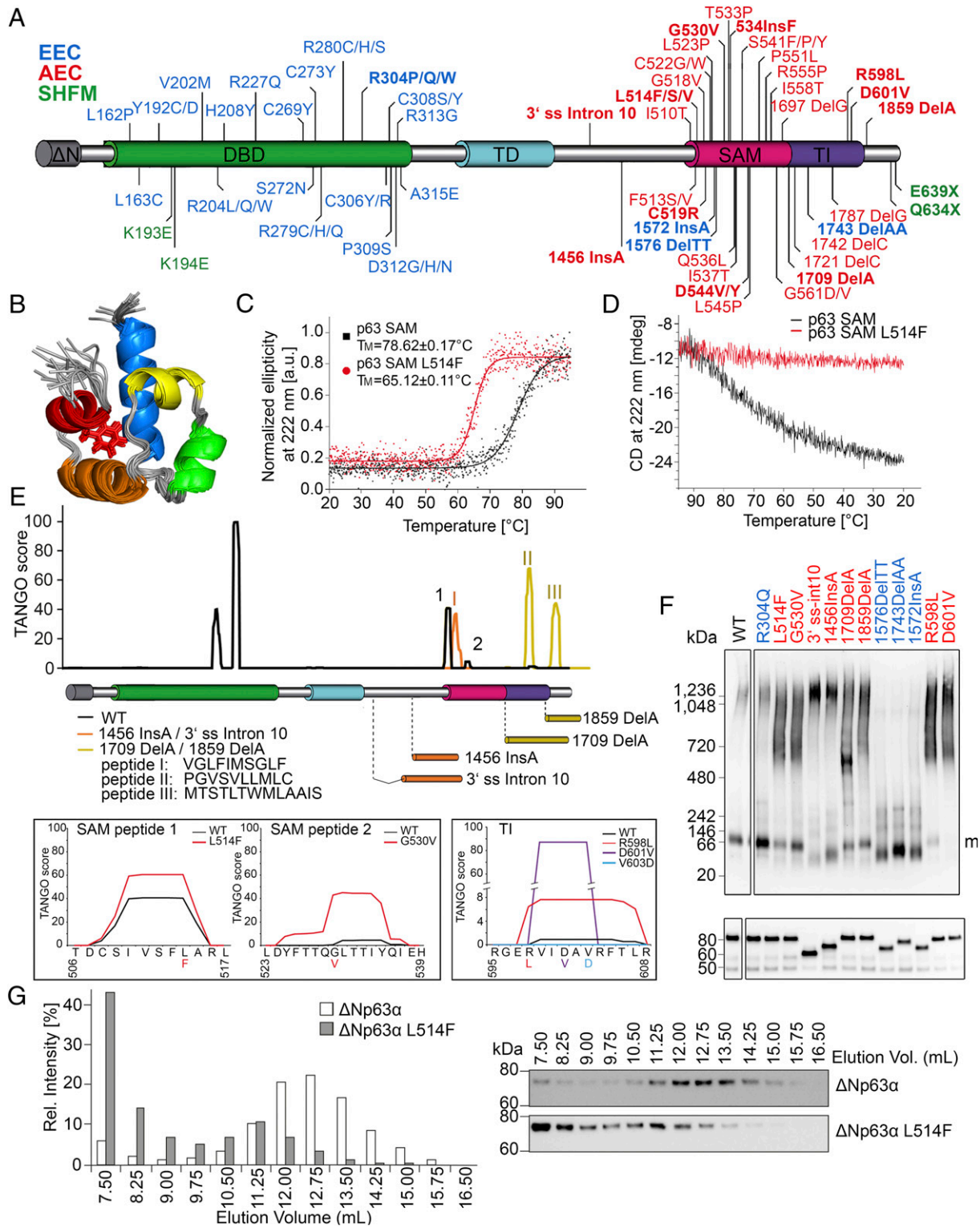

Fig. 1. Aggregation propensity of AEC mutant p63. (*A*) p63 structure and disease-causative mutations (color-coded for each disease as indicated). In bold are mutations used in this study. (*B*) NMR spectroscopy of the murine L514F SAM (PDB ID code 5N2O). Bundle of 20 conformers with the lowest CYANA target function values is shown. The mutated amino acid is indicated as a stick. (*C*) Melting curves of the purified wild-type (black) and L514F (red) SAM domain were recorded by CD spectroscopy. (*D*) Reverse CD melting curves of the purified wild-type and L514F SAM domain after recording the initial melting curve. The mutant remained unfolded due to irreversible precipitation. (*E*) TANGO analysis for the wild-type ΔNp63α (in black) and for the indicated AEC mutations caused by protein elongation (*Upper*: aggregating peptide I-III) or missense mutations in the SAM and TI domains (*Lower*). The V603D variant is predicted to abolish mutant aggregation. (*F*) BN-PAGE (*Upper*) and SDS/PAGE (*Lower*) followed by Western blot for p63 in H1299 extracts expressing wild-type (WT) and the EEC (blue) or the AEC (red) mutations. Soluble ΔNp63α protein runs mainly as a monomer (m). (*G*) SEC followed by Western blot of H1299 cell lysates overexpressing wild-type ΔNp63α and p63L514F mutant. Samples were incubated at 37 °C for 15 min before loading on SEC. Bar diagrams on the *Left* show the relative intensities of each collected fraction.

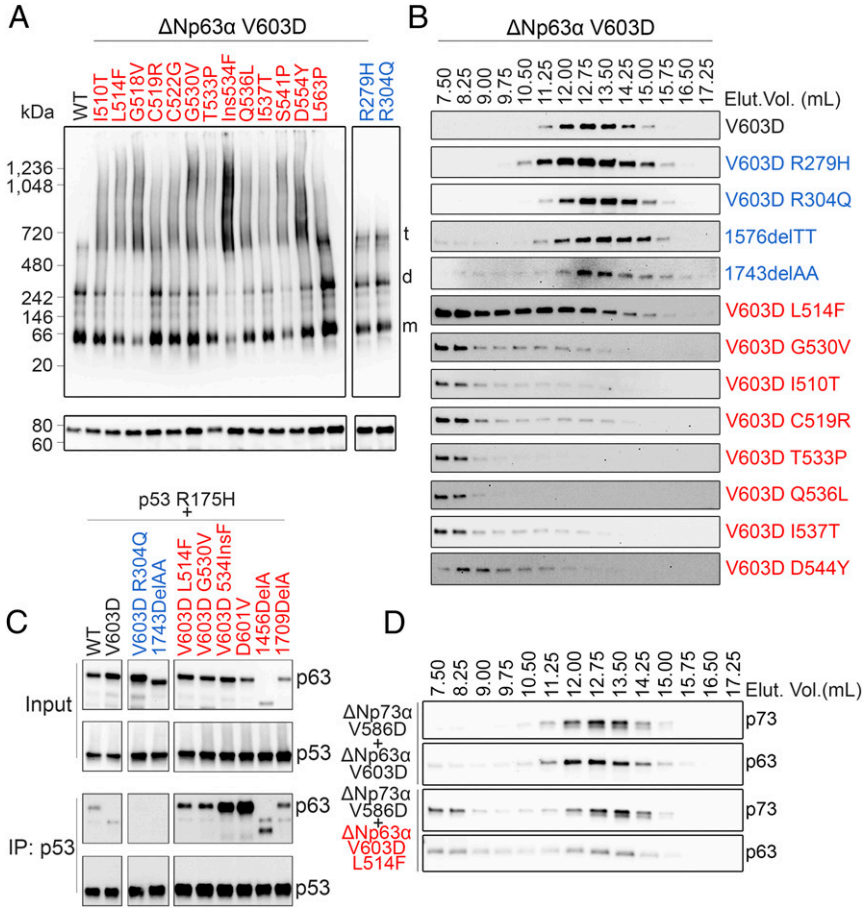

Fig. 2. AEC-associated p63 mutants aggregate with other p53 family members. (*A*) BN-PAGE (*Upper*) and SDS/PAGE (*Lower*) followed by Western blot of the wild-type p63 and an extended set of AEC mutations in the SAM domain in the ΔNp63αV603D variant background (*Left*) and EEC mutant (*Right*) transiently expressed in H1299 cells. (*B*) SEC analysis and Western blot of wild-type and the indicated mutant p63 expressed in H1299 cells. Wild-type ΔNp63α and all EEC mutant proteins elute as tetramers (11.25–15 mL), while AEC mutants are mainly shifted to the void volume (7.5 mL), corresponding to aggregates. (*C*) Coimmunoprecipitation between mutant HA-p53R175H and the indicated Myc-ΔNp63α proteins. p53 was immunoprecipitated (IP) with an HA-specific antibody. Anti-HA Tag antibodies were used to detect p53, whereas anti-Myc antibodies were used for p63. (*D*) SEC analysis and Western blot of ΔNp73α V586D (corresponding to V603D in p63) coexpressed with ΔNp63α V603D either wild-type or L514F in H1299 cells. Samples were incubated at 37 °C for 15 min before loading on SEC.

aggregated with wild-type p63 (*SI Appendix*, Fig. S2*B*), indicating that it may exert a dominant negative function.

As previously shown for wild-type p63 (10, 11), AEC mutant p63 bound p73 (*SI Appendix*, Fig. S2*C*). A p73 mutant protein with no propensity to self-aggregate (p73V586D) (32) aggregated in the presence of mutant p63L514F/V603D, but not with p63V603D alone (Fig. 2*D*). In contrast neither wild-type nor AEC mutant p63 interacted with wild-type p53 (*SI Appendix*, Fig. S2*D*), and no increase in p53 aggregation was observed in the presence of AEC mutant p63 (*SI Appendix*, Fig. S2*E*). Taken together, these data indicate that AEC-associated p63 mutants cause aggregation not only of their wild-type p63 counterpart, but also of wild-type p73, revealing that AEC-associated p63 mutants may display gain-of-function activities through coaggregation with selected family members.

Protein Aggregation Is Associated with Impaired Transcriptional Function in a Mouse Model for AEC Syndrome. To investigate the effect of AEC-associated mutations on ΔNp63α function, we tested the ability of a variety of mutants (Fig. 1*A*) to transactivate the regulatory regions of two crucial p63 target genes, namely keratin 14 (KRT14) and fibroblast growth factor receptor 2 (FGFR2) (15, 34, 35). As previously reported (15, 36), wild-type ΔNp63α efficiently activated the KRT14 promoter as well as the FGFR2 enhancer in HEK293 cells, whereas an EEC causative mutation that directly impairs DNA binding (R304Q) abolished p63 activity (*SI Appendix*, Fig. S3*A*). All tested AEC-associated mutations, including missense mutations in the SAM and TI domains and frameshift mutations, invariably abolished or severely reduced p63 transcriptional activity, whereas two missense mutations in the PS domain causative of SHFM syndrome (Q630X and E635X) retained transactivation activity in this context.

To test whether impaired transcriptional activity of AEC-associated p63 mutants affected its biological function in a more physiological context, we took advantage of a recently developed protocol to convert human dermal fibroblasts (HDFs) into induced keratinocyte-like cells (iKCs) by coexpression of ΔNp63α and Krüppel-like factor 4 (KLF4) (37). Eighteen days after p63/KLF4 transduction, HDFs had converted into iKCs and expressed keratinocyte-specific p63 transcriptional targets, including KRT14 (5, 35), the IFN regulatory factor 6 (IRF6) involved in keratinocyte differentiation (38–40), and desmocollin 3 (DSC3) encoding a desmosome component expressed in basal keratinocytes (14) (Fig. 3 *A* and *B*). In contrast, similarly to the EEC mutant R304Q, AEC mutants were unable to induce expression of keratinocyte-specific target genes, indicating that they are functionally incapable to convert HDFs into iKCs.

To assess whether loss of p63 activity occurs in vivo, we generated a mouse model for AEC syndrome. We have previously shown that a constitutive p63 L514F knock-in mouse phenocopies the clinical

hallmarks of the human disorder at least in part through impaired FGFR2 signaling required for the expansion of epidermal progenitor cells during embryonic development (15, 41). However, the constitutive p63 L514F knock-in mouse line could not be maintained due to fully penetrant cleft palate and consequent perinatal lethality (15). Therefore, we used a conditional knock-in strategy to create L514F mutant mice ($p63^{L514Fflox/L514Fflox}$) in which the AEC-associated mutation L514F is only expressed in the presence of Cre recombinase (Fig. 3 *C* and *D*, and *SI Appendix*, Fig. S3 *B–D*). We first tested the expression of p63 target genes in primary keratinocytes isolated from p63L514F mice infected with an adenovirus carrying the Cre recombinase (Ad-Cre) or a mock control. Target genes previously reported to be positively regulated by p63 and affected in AEC syndrome (14, 15, 35, 40, 42) were strongly reduced in Ad-Cre–infected homozygous keratinocytes and to a lesser extent in heterozygous keratinocytes compared with Ad-GFP controls (Fig. 3 *E* and *F*), confirming that endogenous mutant p63L514F has an impaired transactivation ability. Interestingly, expression of genes repressed by p63, such as Smad7 and Krt8 (5, 17) were derepressed in the presence of the L514F mutant compared with controls (Fig. 3*G*), demonstrating that both transactivation and repression functions of p63 are impaired by AEC mutations.

$p63^{L514Fflox/L514Fflox}$ mice were crossed with K14-Cre knock-in mice carrying the Cre recombinase under the control of the endogenous Krt14 promoter that is active in stratified epithelia from embryonic day 17.5 (43), leading to uniform p63 mutant expression from P0 (Fig. 3*H*). K14-Cre; $p63^{L514Fflox/L514Fflox}$ homozygous mice displayed ectodermal defects and skin erosion typical of AEC syndrome (Fig. 3*I*). Primary keratinocytes isolated from K14-Cre; $p63^{L514Fflox/L514Fflox}$ mice exhibited strongly decreased levels of crucial p63 target genes (Fig. 3*J*).

To test whether mutant p63L514F protein exhibited propensity toward aggregation endogenously, we performed BN-PAGE followed by Western blotting on keratinocyte lysates. As expected, p63 from wild-type keratinocytes mainly runs as a monomer. In contrast, the monomeric form was reduced and large multimeric assemblies were observed in Ad-Cre–infected $p63^{+/L514Fflox}$ keratinocyte lysates, whereas in Ad-Cre–infected $p63^{L514Fflox/L514Fflox}$ keratinocyte lysates, the monomeric form was lost (Fig. 3*K*). Similar results were observed with primary keratinocytes derived from Krt14-Cre;$p63^{+/L514Fflox}$ and Krt14-Cre;$p63^{L514Fflox/L514Fflox}$ mice compared with $p63^{L514Fflox/L514Fflox}$ controls (Fig. 3*L*).

Taken together these data indicate that AEC-associated p63 mutations impair the ability of p63 to act both as a transcriptional activator and as a repressor in vivo, and that the impairment is associated with progressive p63 aggregation in the presence of the mutant form.

Aggregation of AEC-Associated p63 Mutants Causes Impaired DNA Binding. To test whether aggregation of AEC mutants alters the ability of p63 to bind DNA, chromatin immunoprecipitation followed by quantitative PCR (ChIP-qPCR) was performed in HEK293 cells transfected with wild-type and/or mutant p63. As previously reported, the EEC-associated mutant R304Q did not bind to well-characterized p63 genomic binding sites in *KRT14*, and *p63* genes that are positively regulated by p63, or to a p63 binding site in the *CDKN1A* promoter negatively regulated by p63 (3, 5, 15, 44, 45) (Fig. 4*A* and *SI Appendix*, Fig. S4 *A–E*). Surprisingly, even though the AEC mutations do not fall in the DNA binding domain, reduced DNA binding was observed for all AEC-associated mutants, whereas the SHFM-associated mutants efficiently bound DNA. DNA binding was also impaired when wild-type p63 was cotransfected with the L514F mutant, indicating that the mutant exerts a dominant negative effect on p63 DNA binding (Fig. 4*B*). Similarly reduced DNA binding was observed by electrophoretic mobility shift assay (EMSA) in HEK293 nuclear extracts (*SI Appendix*, Fig. S4F).

To assess the physiological relevance of these findings, the ability of p63 to bind DNA was tested in mouse primary keratinocytes within previously characterized p63 binding sites for positively regulated genes (*Irf6*, *Fgfr2*, and *Trp63*) (15, 40, 44) or for a negatively regulated gene *Smad7* (17). A significant reduction in p63 binding to DNA was detected in $p63^{L514Fflox/L514Fflox}$ knock-in keratinocytes, infected with Ad-Cre compared with controls for all tested binding sites (Fig. 4 *C* and *D*). Taken together these data indicate that the ability of p63 to bind DNA is weakened by mutations in the p63 C terminus causative of AEC syndrome.

To evaluate if reduced DNA binding is due to aggregation, we performed DNA pulldown experiments of in vitro translated proteins under conditions in which all mutant and wild-type proteins had a tetrameric conformation and did not form aggregates as assessed by SEC (*SI Appendix*, Fig. S4*G*). While EEC mutants R204W and R304Q had an intrinsic DNA binding impairment, AEC mutants L514F and G530V efficiently bound to DNA at similar levels as the wild-type protein (Fig. 4*E*).

Taken together, these results indicate that the DNA binding ability of AEC mutants is not intrinsically impaired, but rather is weakened, likely due to structural alterations and consequent protein aggregation that occurs in cells.

Transcriptional Activity Is Restored by Reducing the Aggregation Propensity of AEC-Associated Mutant p63. We next investigated whether reversing aggregation would be sufficient to restore transcriptional activity of AEC mutants. To this end we introduced point mutations predicted by TANGO to alleviate aggregation, or we deleted APRs. For the p63L514F mutant, aspartic acids were introduced in each of the two APRs in the SAM domain of the p63L514F mutant (Fig. 1*E*, SAM peptide 1 and 2, *SI Appendix*, Fig. S5*A* and Table S3). Aggregation was alleviated to various extents upon introducing single mutations in either peptide (V511D or F513D for peptide 1, and T533D or I534D for peptide 2), or combinations V511D/I534D, F513D/T533D, and F513D/I534D. Importantly, the double V511D/T533D substitution completely abolished aggregation of the L514F mutant (Fig. 5*A*). Next, we deleted APRs generated by frameshift mutations (Fig. 1*E* and *SI Appendix*, Fig. S1*D*). Deletion of peptide I for the splice mutant 3′ ss-int10, peptide II and III for the 1709DelA, and peptide III for the 1859DelAV603D frameshift mutants completely inhibited their aggregation (Fig. 5*B* and *SI Appendix*, Fig. S5*B*). Finally, we tested the possibility that the V603D mutation could abolish the aggregation propensity of the adjacent mutations R598L or D601V in the TI domain as predicted by TANGO (*SI Appendix*, Fig. S5*A* and Table S2). Introduction of the V603D mutation indeed inhibited aggregation of the R598L or D601V completely or to a large extent, respectively (Fig. 5*C*).

We next used transactivation assays to test whether abolishing aggregation rescued the transcriptional activity of p63 mutants. Consistent with the aggregation data, L514F and L514F/V603D mutants were inactive in luciferase assays, whereas L514F/V603D bearing the V511D/T533D double mutation exhibited restored transcriptional activity (Fig. 5*D*). Similarly, p63 transcriptional activity was fully restored upon deletion of the APRs in the elongated C-terminal domain caused by the frameshift mutations 1709DelA and 1859DelA (Fig. 5*E*). Finally, the V603D variant completely rescued the activity of the two point mutants R598L and D601V in the TI domain (Fig. 5*G*).

The weakened ability of the aggregation mutants to execute transcriptional modulation might explain the disease phenotype observed in AEC patients. To directly test the functional consequence of the increased aggregation for keratinocyte homeostasis, we resorted to the HDF to iKC conversation assay that is otherwise impaired by AEC mutations (Fig. 3 *A* and *B*). Deleting the aggregation peptides of the 1709DelA mutant or introducing V603D into the R598L mutant fully rescued their ability to induce expression of KRT14 and IRF6 in HDF (Fig. 5 *G* and *H*). Similarly, alleviating aggregation of the p63L514F mutant rescued its ability to convert HDF to iKC (Fig. 5*H*).

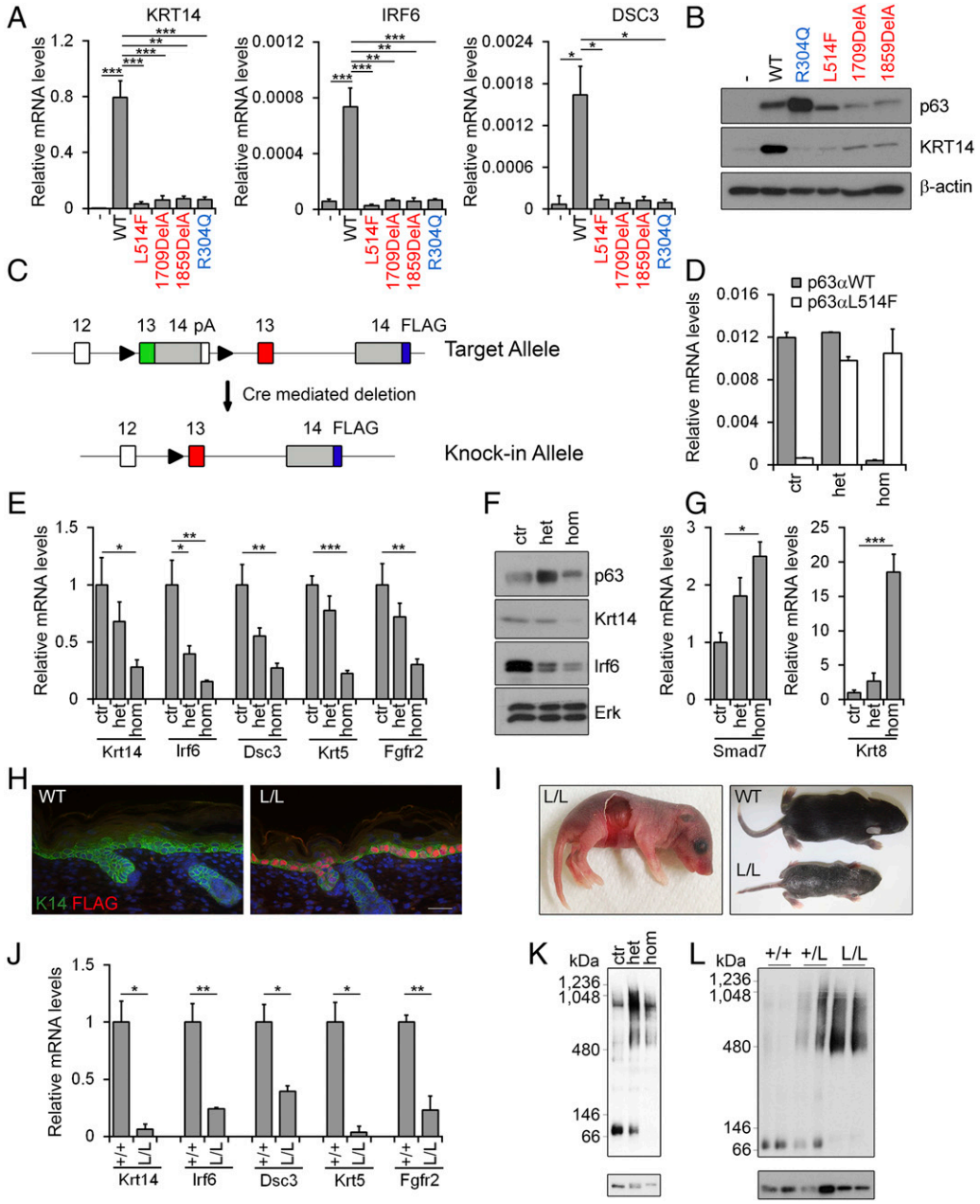

Fig. 3. p63 aggregation and impaired transcriptional function in a mouse model of AEC syndrome. (*A*) Real-time RT-PCR of the indicated keratinocyte-specific p63 target genes in HDFs converted to iKCs by coinfection with Klf4 and the indicated p63 viruses. (*B*) Western blot of Krt14 and p63 in iKCs. β-actin was used as loading control. (*C*) Gene targeting strategy for the $p63^{+/L514Fflox}$ knock-in mice. Mutant exon 13 carrying the L514F mutation is indicated in red. LoxP sites (black triangles) flank wild-type exon 13 (green) fused with the coding portion of exon 14 and the SV40 polyA (pA). 3xFLAG (blue) was placed at the end of the coding sequence in exon 14. FLAG-tagged p63 mutant protein is expressed upon Cre mediated deletion. (*D*) Real-time RT-PCR of wild-type p63 (gray bars) and p63L514F (white bars) in keratinocytes derived from $p63^{+/floxL514F}$ (het) and $p63^{L514Fflox/L514Fflox}$ (hom) mice after Ad-Cre–mediated deletion or after infection with Ad-GFP (ctr). (*E*) Real-time RT-PCR of target genes induced by p63 in mutant keratinocytes with ctr levels set to 1 ($n = 5$). (*F*) Western blot for p63 and the protein products of its target genes Krt14 and Irf6 in mutant keratinocytes. ERK was used as loading control. (*G*) Real-time RT-PCR of p63 repressed target genes in mutant keratinocytes ($n = 3$). (*H*) Immunofluorescence for K14 (green) and FLAG-tagged p63L514F (red) in epidermis of wild-type (WT) and K14-Cre; $p63^{L514Fflox/L514Fflox}$ (L/L) mice at P0. (Scale bars: 50 μm.) (*I*) Macroscopic phenotype of L/L mutant mice. Approximately 10% of newborn mice displayed large areas of skin erosions (*Left*). Skin crusting and ulcerations with reduced body size and dehydration were observed at P7-P8 in 100% of mutant mice (*Right*). (*J*) Real-time RT-PCR of p63 target genes in +/+ and L/L epidermis ($n = 6$). (*K*) BN-PAGE (*Upper*) and SDS/PAGE (*Lower*) followed by Western blot for p63 in mouse primary keratinocytes infected with Ad-Cre or Ad-GFP as in *D*. (*L*) BN-PAGE (*Upper*) and SDS/PAGE (*Lower*) followed by Western blot for p63 in primary keratinocytes isolated from mice with the indicated genotypes. Data are shown as mean ± SEM with the exception of *D* in which error bars indicate SD. Statistical significance was assessed using paired two-tailed *t* test (*J*) and one-way ANOVA analysis (*A*, *E*, and *G*). $*P \leq 0.05$; $**P \leq 0.001$; $***P \leq 0.0001$.

Finally, when exogenously expressed in wild-type keratinocytes, deleterious mutants p63L514F and p63R598L led to partial p63 aggregation and induction of Krt8 expression, a marker of simple epithelial tissues repressed by wild-type p63 and aberrantly expressed in knock-in mutant keratinocytes (Fig. 3*G*) (5). Importantly, p63 aggregation and Krt8 expression were suppressed by expression of rescue mutants (p63L514FV603D/V511D/T533D and R598LV603D) (*SI Appendix*, Fig. S5 *C* and *D*).

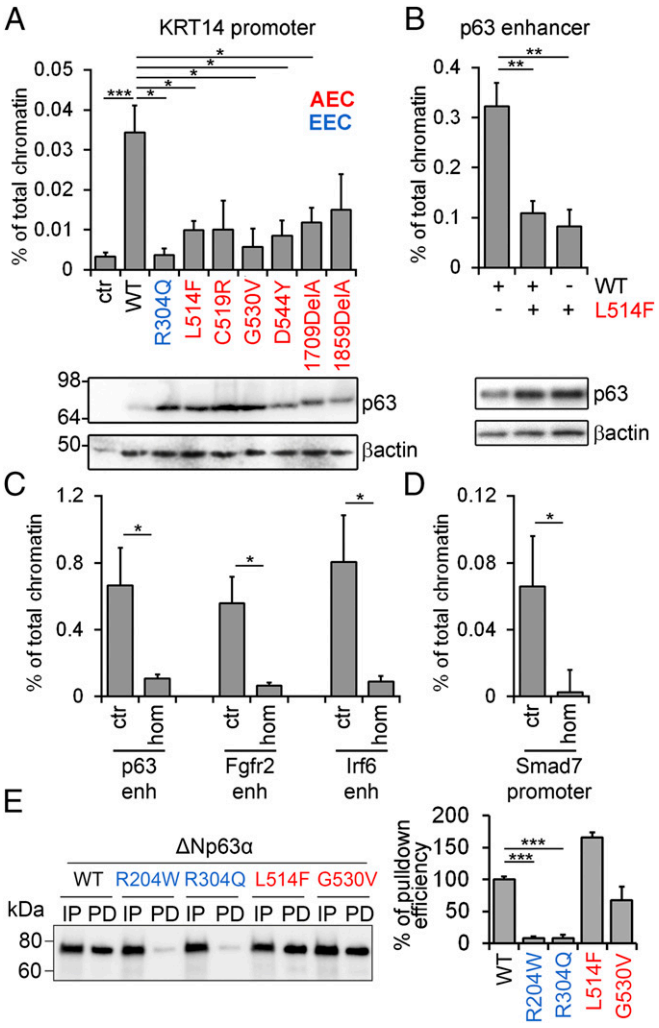

Fig. 4. AEC-associated p63 mutant proteins exhibit impaired DNA binding in cells. (*A*) ChIP-qPCR of the KRT14 promoter from HEK293 cells overexpressing p63 wild-type (WT) and the indicated mutants ($n = 6$) (*Upper*) and SDS/PAGE (*Lower*) followed by Western blot for p63 and β-actin (*Lower*). (*B*) ChIP-qPCR of the p63 enhancer from HEK293 cells cotransfected with p63 WT and p63L514F ($n = 5$) and relative SDS/PAGE (*Lower*) as in *A*. (*C*) ChIP-qPCR of the indicated p63-responsive enhancers in primary keratinocytes derived from $p63^{L514Fflox/L514Fflox}$ (hom) mice infected with Ad-Cre. Keratinocytes infected with Ad-GFP were used as controls (ctr) ($n = 4$). (*D*) ChIP-qPCR of the indicated p63-repressed gene element in primary keratinocytes under conditions as in *C* ($n = 3$). (*E*) Pulldown (PD) assay and Western blot of in vitro translated p63 with immobilized DNA oligonucleotides corresponding to the p63 responsive element on the human CDKN1A promoter. Input (IP). Percentage of pulldown efficiency is shown in the *Right* ($n = 3$). Data are shown as mean ± SEM with the exception of *E* in which error bars indicate SD. Statistical significance was assessed using paired two-tailed *t* test (*C* and *D*) and one-way ANOVA (*A*, *B*, and *E*). $*P \leq 0.05$; $**P \leq 0.001$; $***P \leq 0.0001$.

Taken together, these data indicate that missense mutations in the SAM domain or TI domain, or frameshift mutations leading to AEC syndrome, cause p63 protein aggregation and loss of transcriptional activity. Alleviating aggregation by mutating or removing amino acids responsible for the aggregation is sufficient to restore p63 transcriptional function.

Discussion

Among the p63-associated disorders, AEC syndrome is uniquely characterized by long-lasting and life-threatening skin erosions. Despite the severity of the symptoms, molecular studies have been hampered by the paucity of human biological material, and the poor understanding of the molecular mechanisms underlying the disorder. Here, we have shown that *p63* mutations associated with AEC syndrome cause reduced DNA binding and transcriptional activity due to mutant protein aggregation. Aggregation is caused by either aberrant protein elongation introducing aggregation-prone peptides, enhancing the intrinsic low APR of the TI domain, or by conformational changes that expose peptides with a natural high aggregation propensity. The latter is equivalent to the well-known gain-of-function mutations of p53 in cancer (e.g., R175H). AEC-associated p63 mutant proteins coaggregate with their wild-type counterpart and with p73. Importantly, the aggregation can be reversed and transcriptional activity of p63 rescued upon the introduction of specific point mutations that disrupt aggregation-prone peptides or upon their deletion.

To determine the relevance of these findings in vivo, we utilized a newly developed mouse model for AEC syndrome. We showed that endogenous mutant p63 in AEC mouse keratinocytes exhibits aberrant aggregation and inactivation of both transcriptional activating and repressing functions. This suggests that AEC mutations are unlikely to selectively impair interactions between p63 and specific coactivators or corepressors, but rather cause protein conformational changes that alter p63 function. The partial impairment in DNA binding observed for AEC mutants indicates that the propensity to form aggregates affects p63 affinity for DNA. This impairment, however, is not an intrinsic property of the AEC mutants but rather an indirect consequence of aggregation. DNA binding impairment therefore depends on the degree of aggregation and the effective removal of aggregates. This might partially explain differences in severity of the symptoms observed in different patients bearing the same mutation (25, 46), and differences in severity between patients diagnosed with AEC syndrome and Rapp–Hodgkin syndrome (OMIM 129400), diseases that have been suggested to be variable manifestations of the same clinical entity caused by overlapping p63 mutations in the carboxyl terminal domain (47, 48).

Aggregating proteins can inactivate other proteins through coaggregation. Three categories of proteins affected by mutant p63 can be distinguished. The first is wild-type p63 that exists in heterozygous AEC patients. Due to the ability to form tetramers through the tetramerization domain, mutant p63 can form complexes with wild-type p63. Formation of aggregates by the mutant protein also draws wild-type p63 into larger aggregates, thus exerting a dominant negative effect. This effect was confirmed in our experiments by showing that mutant p63 in L514F heterozygous keratinocytes acts as a dominant negative inhibitor of wild-type p63 function. The second category includes other p63 binding partners. One example is the family member p73, which can form heterotetramers with p63, consisting of one p63 dimer and one p73 dimer. Structural studies have shown that p63/p73 heterotetramers are thermodynamically more stable than either homotetramer (49). Although the function of p63/p73 interactions in skin biology remains uncharacterized, both proteins are expressed simultaneously in the basal layer of the epidermis. While p63 is abundant in all cells, p73 is more highly expressed in the frequently dividing stem cell population (49, 50). The third category includes proteins that normally do not interact or interact very weakly with wild-type p63 but, due to the existence of hydrophobic patches, can coaggregate with aggregating mutant p63. One example is p53R175H, a structural mutant with gain-of-function properties that interacts with specific isoforms of p73 and, to a lesser extent, of p63, interfering with their functions (32, 51, 52). The p53R175H mutant interacts very weakly with wild type ΔNp63α (refs. 32 and 51 and present study), whereas it interacts strongly with AEC mutants. The biological significance of this interaction remains to be determined. Since p63 is an abundantly expressed transcription factor in keratinocytes, and AEC mutants often show a longer half-life in cells than the wild-type protein (36), mutant

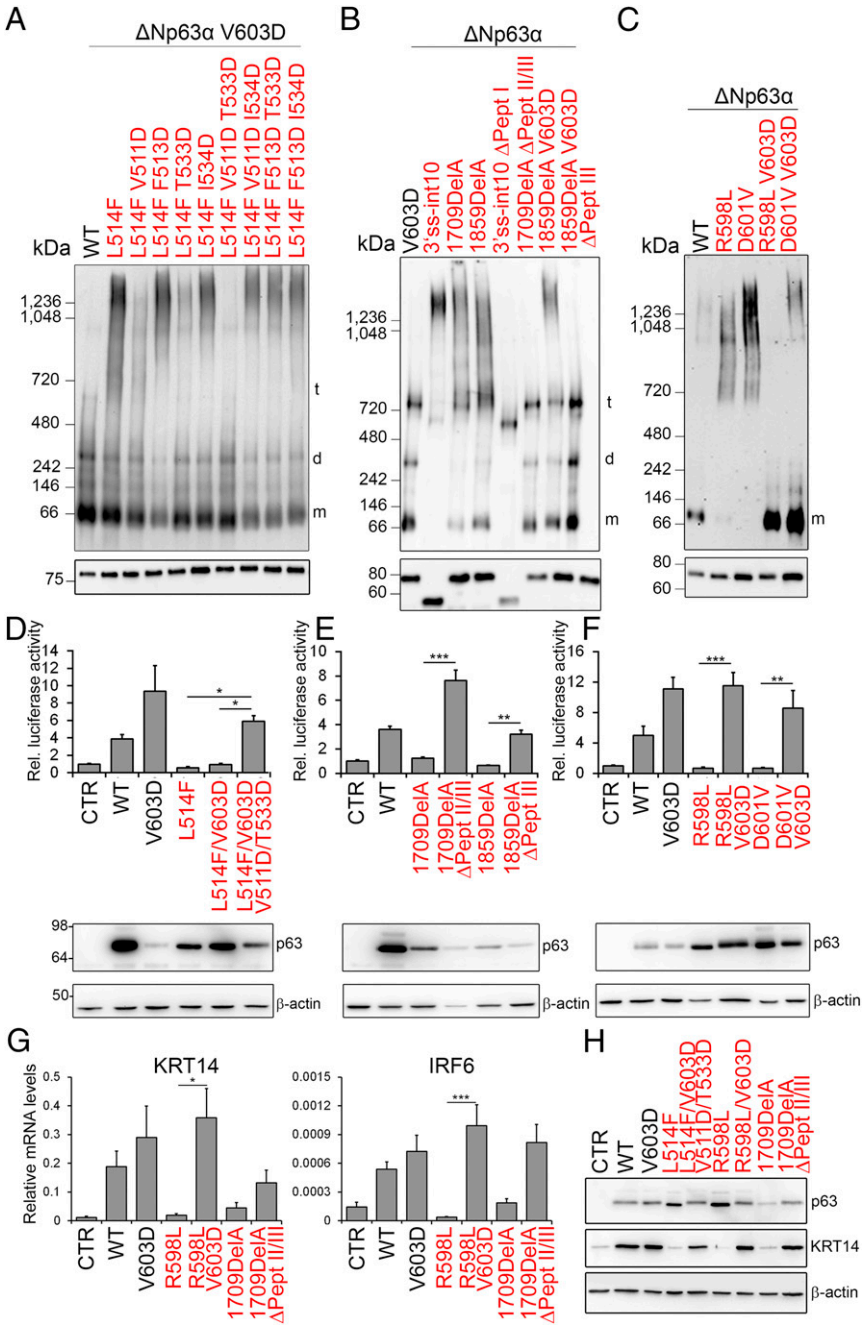

Fig. 5. Transcriptional activity is restored by reducing the aggregation propensity of AEC-associated mutant p63. (*A–C*) BN-PAGE (*Upper*) and SDS/PAGE (*Lower*) followed by Western blot of p63 and the indicated mutations and deletions transfected in HEK 293 cells. (*D–F*) Luciferase reporter assays of wild-type and mutant p63 on the KRT14 promoter in HEK293 cells ($n = 3$) (*Upper*). Luciferase data were normalized for *Renilla* luciferase activity. SDS/PAGE (*Lower*) followed by Western blot of wild-type and mutant p63 are shown as control. (*G*) Real-time RT-PCR of the indicated keratinocyte-specific p63 target genes in HDFs converted to iKCs by coinfection with KLF4 and the indicated p63 viruses. (*H*) Western blot of KRT14 and p63 in iKCs. β-actin was used as loading control. Data are shown as mean ± SEM, and statistical significance was assessed using one-way ANOVA analysis. $^*P \leq 0.05$; $^{**}P \leq 0.001$; $^{***}P \leq 0.0001$.

p63 may be able to sequester other nuclear proteins. Aggregation between AEC mutants and p73 and/or other p63 protein partners helps explain the severe skin phenotype specifically observed in AEC syndrome and not in other diseases associated with p63 mutations. Future studies should focus on identifying nuclear proteins that may form large, inactive complexes with mutant p63. By revealing that AEC syndrome is a protein aggregation disorder and that aggregation can be reverted leading to a functional rescue, our studies open avenues for therapeutic intervention.

Materials and Methods

Detailed descriptions are provided in *SI Appendix*.

Mice. K14-Cre (Krt14-CreΔneo) knock-in mice were obtained from J. Huelsken, Swiss Institute for Experimental Cancer Research, Lausanne, Switzerland, and were used to induce expression of the p63 mutant protein in stratified epithelia at late stages of embryonic development (43). See *SI Appendix* for the conditional knock-in mice ($p63^{+/L514Fflox}$) generation. All mouse work was conducted at CEINGE according to the Italian ethical regulations under the animal license 311/2016-PR.

Coimmunoprecipitation, SDS/PAGE, BN-PAGE. For coimmunoprecipitation, cells were lysed in RIPA lysis buffer [20 mM Tris·HCl (pH 7.5), 150 mM NaCl, 1 mM Na_2EDTA, 1 mM EGTA, 1% Nonidet P-40, 1% sodium deoxycholate, 1 mM DTT] with the addition of protease and phosphatase inhibitors. Lysates were cleared by centrifugation and incubated with 2 μg of HA-antibody, p73 antibody, or normal IgG overnight at 4 °C. The immunocomplexes were purified with 25 μL of Protein G Dynabeads (Thermo Fisher Scientific) for 3 h at 4 °C. For SDS/PAGE, cells were loaded in Laemmli sample buffer with 5% β-mercaptoethanol. For BN-PAGE, cells were lysed in native lysis buffer [25 mM Tris (pH 7.5), 150 mM NaCl, 2 mM $MgCl_2$, 20 mM CHAPS, 1 mM DTT and protease inhibitors]. Collected cells were incubated 1 h on ice in the presence of benzonase (Merck Millipore). Protein extracts were then mixed with 20% Glycerol and 5 mM Coomassie G-250 and loaded on 3–12% Novex Bis-Tris gradient gel for BN-PAGE (Thermo Fisher Scientific). Antibodies used in this study are listed in *SI Appendix*, Table S5.

Analytical SEC. Analytical SEC experiments were performed as previously described (9, 32). Briefly, either a Superose 6 PC 3.2/300 column (GE Healthcare) for in vitro translated p63 or a Superose 6 GL 10/300 column (GE Healthcare) for cell lysates of transiently transfected H1299 cells were used. H1299 cell lysate was prepared by three cycles of freezing and thawing in SEC running buffer (50 mM Tris pH 7.5; 150 mM NaCl; 1 mM DTT) with protease inhibitors and Benzonase followed by removal of cell debris by centrifugation. Before injection, cell lysates were incubated at 37 °C for 15 min. The Superose 6 GL 10/300 column was calibrated using the Gel Filtration HMW and LMW Calibration Kits.

RNA Isolation, RT-qPCR, and ChIP-qPCR. For RT-qPCR, total RNA was extracted using TRIzol reagent (Thermo Fisher Scientific) and cDNA was synthesized using SuperScript Vilo, Real time RT-PCR was performed using the SYBR Green PCR master mix (Thermo Fisher Scientific) in an ABI PRISM 7500 (Thermo Fisher Scientific). Target genes were quantified using specific oligonucleotide primers (*SI Appendix*, Table S4) and normalized for mouse β-actin or human RPLP0 expression. For ChIP-qPCR, chromatin was immunoprecipitated as previously reported (44). Immunoprecipitation was performed using rabbit antibodies for p63 or rabbit IgG as control. Bound chromatin was purified with Protein A Sepharose (GE Healthcare) for 1 h at 4 °C. Bound DNA was quantified by real-time PCR using specific oligonucleotide primers (*SI Appendix*, Table S4) and normalized to input.

CD Melting Curve. CD melting curves of p63 SAM or L514F mutant were recorded with Jasco J-810 spectropolarimeter (Jasco Labortechnik). Changes in CD signal at 222 nm and dynode voltage were recorded from 20 °C to 95 °C and backward from 95 °C to 20 °C. Melting curves were corrected for the pretransition phase and melting points were acquired using the Boltzman sigmoidal fit function (Origin Pro-9.1G). To follow turbidity as an indicator of precipitation and aggregation during unfolding, the dynode voltage was plotted against the temperature as described before (53).

DNA Pulldown Assay. Oligonucleotides used for the DNA pulldown assay correspond to the p53/p63/p73 binding site on the CDKN1A promoter (9). Biotinylated annealed DNA strands were immobilized on streptavidin agarose beads (GE Healthcare) in pulldown buffer (50 mM Tris pH 8.0; 150 mM NaCl; 0.1% Tween-20), incubated with in vitro translated p63 and washed four times with pulldown buffer. Bound p63 was eluted with boiling sample buffer and pulldown efficiency was analyzed by Western blot.

NMR Spectroscopy and Structure Determination. All spectra were recorded at 296 K on Bruker Avance spectrometers (proton frequencies of 600 MHz and 800 MHz) equipped with cryo-probes. The NMR structure of the murine p63 SAM L514F mutant was obtained using combined automated NOE assignment and structure calculation (54) with the program package CYANA (55). An overview of the structural statistics is given in *SI Appendix*, Table S1. Details about the recorded spectra and structure calculation are described in *SI Appendix*. The accession number for the coordinates and structures factors of murine p63 SAM L514F mutant reported in this manuscript is PDB ID code 5N2O.

Quantification and Statistical Analysis. All datasets derive from at least three independent experiments unless otherwise indicated. The number of independent experiments are indicated (*n*), with the exception of Fig. 3*J* in which *n* indicate number of analyzed animals. Data are presented as the mean of independent experiments ±SEM or SD as indicated. All statistical analyses were performed using GraphPad Prism software (version 7.0). In experiments comparing two samples, paired or unpaired, two-tailed *t* testing was performed, whereas when comparing multiple independent samples, one-way analysis of variance (ANOVA) followed by Tukey's HSD multiple comparison post hoc tests were performed as described in the figure legends. *P* values of statistical significance are represented as $*P \leq 0.05$; $**P \leq 0.01$; $***P \leq 0.001$.

ACKNOWLEDGMENTS. We thank Anna Mandinova for critical reading of the manuscript and helpful discussion; George Sen for helpful discussion on the HDF-to-iKC conversion assay; Eleonora Candi, Bert Vogelstein, and Adele Abbate (Reithera Srl) for reagents; Dario Acampora (Institute of Genetics and Biophysics "A. Buzzati Traverso") for generating mice; Annamaria Carissimo and the Telethon Institute of Genetics and Medicine Bioinformatics Core for assistance in the statistical analysis; and Maria Rosaria Mollo for the initial mouse characterization. We appreciate language and content editing assistance provided by DerMEDit. This work was supported by Telethon Grants GGP09230 and GGP16235 (to C.M.), ERA-Net Research Program on Rare Diseases (ERARE-2) Skin-Dev (C.M.), Italian Association for Cancer Research Grant IG2011-N.11369 (to C.M.), Fondation Dind-Cottier pour la recherche sur la peau (C.M.), DFG Grant DO 545/8-1 (to V.D.), the Centre for Biomolecular Magnetic Resonance, and the Cluster of Excellence Frankfurt (Macromolecular Complexes). P.G. is supported by a Lichtenberg Professorship of the Volkswagen Foundation. C.R. is a PhD student in molecular oncology at the European School of Molecular Medicine.

1. Koster MI, Kim S, Mills AA, DeMayo FJ, Roop DR (2004) p63 is the molecular switch for initiation of an epithelial stratification program. *Genes Dev* 18:126–131.
2. Mills AA, et al. (1999) p63 is a p53 homologue required for limb and epidermal morphogenesis. *Nature* 398:708–713.
3. Nguyen BC, et al. (2006) Cross-regulation between Notch and p63 in keratinocyte commitment to differentiation. *Genes Dev* 20:1028–1042.
4. Senoo M, Pinto F, Crum CP, McKeon F (2007) p63 Is essential for the proliferative potential of stem cells in stratified epithelia. *Cell* 129:523–536.
5. Truong AB, Kretz M, Ridky TW, Kimmel R, Khavari PA (2006) p63 regulates proliferation and differentiation of developmentally mature keratinocytes. *Genes Dev* 20:3185–3197.
6. Yang A, et al. (1999) p63 is essential for regenerative proliferation in limb, craniofacial and epithelial development. *Nature* 398:714–718.
7. Vanbokhoven H, Melino G, Candi E, Declercq W (2011) p63, a story of mice and men. *J Invest Dermatol* 131:1196–1207.
8. Yang A, et al. (1998) p63, a p53 homolog at 3q27-29, encodes multiple products with transactivating, death-inducing, and dominant-negative activities. *Mol Cell* 2: 305–316.
9. Deutsch GB, et al. (2011) DNA damage in oocytes induces a switch of the quality control factor TAp63α from dimer to tetramer. *Cell* 144:566–576.
10. Coutandin D, et al. (2009) Conformational stability and activity of p73 require a second helix in the tetramerization domain. *Cell Death Differ* 16:1582–1589.
11. Rocco JW, Leong CO, Kuperwasser N, DeYoung MP, Ellisen LW (2006) p63 mediates survival in squamous cell carcinoma by suppression of p73-dependent apoptosis. *Cancer Cell* 9:45–56.
12. Suh EK, et al. (2006) p63 protects the female germ line during meiotic arrest. *Nature* 444:624–628.
13. Crum CP, McKeon FD (2010) p63 in epithelial survival, germ cell surveillance, and neoplasia. *Annu Rev Pathol* 5:349–371.
14. Ferone G, et al. (2013) p63 control of desmosome gene expression and adhesion is compromised in AEC syndrome. *Hum Mol Genet* 22:531–543.
15. Ferone G, et al. (2012) Mutant p63 causes defective expansion of ectodermal progenitor cells and impaired FGF signalling in AEC syndrome. *EMBO Mol Med* 4:192–205.
16. Antonini D, et al. (2010) Transcriptional repression of miR-34 family contributes to p63-mediated cell cycle progression in epidermal cells. *J Invest Dermatol* 130: 1249–1257.
17. De Rosa L, et al. (2009) p63 Suppresses non-epidermal lineage markers in a bone morphogenetic protein-dependent manner via repression of Smad7. *J Biol Chem* 284: 30574–30582.
18. LeBoeuf M, et al. (2010) Hdac1 and Hdac2 act redundantly to control p63 and p53 functions in epidermal progenitor cells. *Dev Cell* 19:807–818.
19. Ramsey MR, He L, Forster N, Ory B, Ellisen LW (2011) Physical association of HDAC1 and HDAC2 with p63 mediates transcriptional repression and tumor maintenance in squamous cell carcinoma. *Cancer Res* 71:4373–4379.
20. Cicero DO, et al. (2006) NMR structure of the p63 SAM domain and dynamical properties of G534V and T537P pathological mutants, identified in the AEC syndrome. *Cell Biochem Biophys* 44:475–489.
21. McGrath JA, et al. (2001) Hay-Wells syndrome is caused by heterozygous missense mutations in the SAM domain of p63. *Hum Mol Genet* 10:221–229.
22. Chi SW, Ayed A, Arrowsmith CH (1999) Solution structure of a conserved C-terminal domain of p73 with structural homology to the SAM domain. *EMBO J* 18:4438–4445.
23. Coutandin D, et al. (2016) Quality control in oocytes by p63 is based on a spring-loaded activation mechanism on the molecular and cellular level. *Elife* 5:e13909.
24. Straub WE, et al. (2010) The C-terminus of p63 contains multiple regulatory elements with different functions. *Cell Death Dis* 1:e5.

25. Rinne T, Hamel B, van Bokhoven H, Brunner HG (2006) Pattern of p63 mutations and their phenotypes–Update. *Am J Med Genet A* 140:1396–1406.
26. Celli J, et al. (1999) Heterozygous germline mutations in the p53 homolog p63 are the cause of EEC syndrome. *Cell* 99:143–153.
27. Julapalli MR, Scher RK, Sybert VP, Siegfried EC, Bree AF (2009) Dermatologic findings of ankyloblepharon-ectodermal defects-cleft lip/palate (AEC) syndrome. *Am J Med Genet A* 149A:1900–1906.
28. Ianakiev P, et al. (2000) Split-hand/split-foot malformation is caused by mutations in the p63 gene on 3q27. *Am J Hum Genet* 67:59–66.
29. Payne AS, et al. (2005) Two novel TP63 mutations associated with the ankyloblepharon, ectodermal defects, and cleft lip and palate syndrome: A skin fragility phenotype. *Arch Dermatol* 141:1567–1573.
30. Sathyamurthy A, Freund SM, Johnson CM, Allen MD, Bycroft M (2011) Structural basis of p63α SAM domain mutants involved in AEC syndrome. *FEBS J* 278:2680–2688.
31. Fernandez-Escamilla AM, Rousseau F, Schymkowitz J, Serrano L (2004) Prediction of sequence-dependent and mutational effects on the aggregation of peptides and proteins. *Nat Biotechnol* 22:1302–1306.
32. Kehrloesser S, et al. (2016) Intrinsic aggregation propensity of the p63 and p73 TI domains correlates with p53R175H interaction and suggests further significance of aggregation events in the p53 family. *Cell Death Differ* 23:1952–1960.
33. Xu J, et al. (2011) Gain of function of mutant p53 by coaggregation with multiple tumor suppressors. *Nat Chem Biol* 7:285–295.
34. Candi E, et al. (2007) DeltaNp63 regulates thymic development through enhanced expression of FgfR2 and Jag2. *Proc Natl Acad Sci USA* 104:11999–12004.
35. Romano RA, Birkaya B, Sinha S (2007) A functional enhancer of keratin14 is a direct transcriptional target of deltaNp63. *J Invest Dermatol* 127:1175–1186.
36. Browne G, et al. (2011) Differential altered stability and transcriptional activity of ΔNp63 mutants in distinct ectodermal dysplasias. *J Cell Sci* 124:2200–2207.
37. Chen Y, Mistry DS, Sen GL (2014) Highly rapid and efficient conversion of human fibroblasts to keratinocyte-like cells. *J Invest Dermatol* 134:335–344.
38. Ingraham CR, et al. (2006) Abnormal skin, limb and craniofacial morphogenesis in mice deficient for interferon regulatory factor 6 (Irf6). *Nat Genet* 38:1335–1340.
39. Richardson RJ, et al. (2006) Irf6 is a key determinant of the keratinocyte proliferation-differentiation switch. *Nat Genet* 38:1329–1334.
40. Thomason HA, et al. (2010) Cooperation between the transcription factors p63 and IRF6 is essential to prevent cleft palate in mice. *J Clin Invest* 120:1561–1569.
41. Petiot A, et al. (2003) A crucial role for Fgfr2-IIIb signalling in epidermal development and hair follicle patterning. *Development* 130:5493–5501.
42. Romano RA, Ortt K, Birkaya B, Smalley K, Sinha S (2009) An active role of the DeltaN isoform of p63 in regulating basal keratin genes K5 and K14 and directing epidermal cell fate. *PLoS One* 4:e5623.
43. Huelsken J, Vogel R, Erdmann B, Cotsarelis G, Birchmeier W (2001) beta-Catenin controls hair follicle morphogenesis and stem cell differentiation in the skin. *Cell* 105:533–545.
44. Antonini D, et al. (2015) A composite enhancer regulates p63 gene expression in epidermal morphogenesis and in keratinocyte differentiation by multiple mechanisms. *Nucleic Acids Res* 43:862–874.
45. Kouwenhoven EN, et al. (2010) Genome-wide profiling of p63 DNA-binding sites identifies an element that regulates gene expression during limb development in the 7q21 SHFM1 locus. *PLoS Genet* 6:e1001065.
46. Rinne T, Bolat E, Meijer R, Scheffer H, van Bokhoven H (2009) Spectrum of p63 mutations in a selected patient cohort affected with ankyloblepharon-ectodermal defects-cleft lip/palate syndrome (AEC). *Am J Med Genet A* 149A:1948–1951.
47. Bertola DR, et al. (2004) Molecular evidence that AEC syndrome and Rapp-Hodgkin syndrome are variable expression of a single genetic disorder. *Clin Genet* 66:79–80.
48. Clements SE, et al. (2010) Rapp-Hodgkin and Hay-Wells ectodermal dysplasia syndromes represent a variable spectrum of the same genetic disorder. *Br J Dermatol* 163:624–629.
49. Gebel J, et al. (2016) Mechanism of TAp73 inhibition by ΔNp63 and structural basis of p63/p73 hetero-tetramerization. *Cell Death Differ* 23:1930–1940.
50. Sada A, et al. (2016) Defining the cellular lineage hierarchy in the interfollicular epidermis of adult skin. *Nat Cell Biol* 18:619–631.
51. Gaiddon C, Lokshin M, Ahn J, Zhang T, Prives C (2001) A subset of tumor-derived mutant forms of p53 down-regulate p63 and p73 through a direct interaction with the p53 core domain. *Mol Cell Biol* 21:1874–1887.
52. Lang GA, et al. (2004) Gain of function of a p53 hot spot mutation in a mouse model of Li-Fraumeni syndrome. *Cell* 119:861–872.
53. Benjwal S, Verma S, Rohm KH, Gursky O (2006) Monitoring protein aggregation during thermal unfolding in circular dichroism experiments. *Protein Sci* 15:635–639.
54. Güntert P, Buchner L (2015) Combined automated NOE assignment and structure calculation with CYANA. *J Biomol NMR* 62:453–471.
55. Güntert P, Mumenthaler C, Wüthrich K (1997) Torsion angle dynamics for NMR structure calculation with the new program DYANA. *J Mol Biol* 273:283–298.